

Lattice distortions and the metal–insulator transition in pure and Ti-substituted $\text{Ca}_3\text{Ru}_2\text{O}_7$

V Petkov^{1,*} , T Durga Rao^{1,2}, A Zafar¹, A M Milinda Abeykoon³, E Fletcher⁴ , J Peng⁵, Z Q Mao⁶ and X Ke⁴

¹ Department of Physics, Central Michigan University, Mt. Pleasant, MI 48858, United States of America

² Department of Physics, GITAM, Visakhapatnam, Andhra Pradesh 530045, India

³ Photon Sciences Division, Brookhaven National Laboratory, Upton, NY 11973, United States of America

⁴ Department Physics and Astronomy, Michigan State University, East Lansing, MI 48824, United States of America

⁵ School of Physics, Southeast University, Nanjin, People's Republic of China

⁶ Department of Physics, Pennsylvania State University, University Park, State College, PA 16802, United States of America

E-mail: petko1vg@cmich.edu

Received 13 September 2022, revised 15 October 2022

Accepted for publication 26 October 2022

Published 8 November 2022



CrossMark

Abstract

We report pair distribution function studies on the relationship between the metal–insulator transition (MIT) and lattice distortions in pure and Ti-substituted bilayer $\text{Ca}_3\text{Ru}_2\text{O}_7$. Structural refinements performed as a function of temperature, magnetic field and length scale reveal the presence of lattice distortions not only within but also orthogonal to the bilayers. Because of the distortions, the local and average crystal structure differ across a broad temperature region extending from room temperature to temperatures below the MIT. The coexistence of distinct lattice distortions is likely to be behind the marked structural flexibility of $\text{Ca}_3\text{Ru}_2\text{O}_7$ under external stimuli. This observation highlights the ubiquity of lattice distortions in an archetypal Mott system and calls for similar studies on other families of strongly correlated materials.

Supplementary material for this article is available [online](#)

Keywords: lattice, distortions, metal–insulator transition, strongly correlated systems

(Some figures may appear in colour only in the online journal)

1. Introduction

Strongly correlated transition metal oxides are known to exhibit unconventional properties due to the presence of strongly interacting charge, spin and lattice degrees of freedom [1–4]. Moreover, the interaction renders their ground state susceptible to external stimuli, providing an opportunity to

investigate the former by tuning the latter. A typical example is the family of Ruddelsden–Popper type layered calcium rutenates, in particular the bilayer compound $\text{Ca}_3\text{Ru}_2\text{O}_7$ and its derivatives [5–9]. It is built of perovskite $(\text{CaRuO}_3)_2$ bilayers with RuO_6 octahedra that are separated by CaO rock-salt layers, as shown in figure 1 [10]. Due to the small Goldschmidt's tolerance factor [11], the compound exhibits RuO_6 octahedral rotations and tilts, contributing to its structural flexibility. It is paramagnetic (PM) at room temperature and becomes an antiferromagnet (AFM) at $T_N = 56$ K while

* Author to whom any correspondence should be addressed.

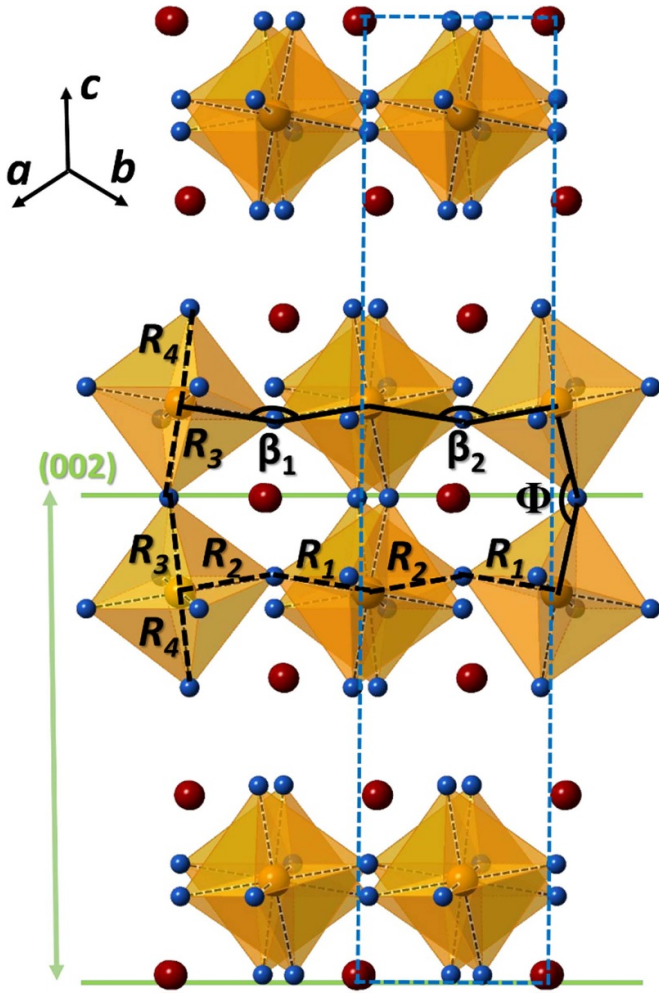


Figure 1. Fragment from the crystal structure of $\text{Ca}_3\text{Ru}_2\text{O}_7$ built of double layers of Ru-O₆ octahedra (brown) with Ca atoms (red) occupying empty space between the octahedra. The octahedra are both in-plane rotated and out-of-plane tilted with respect to one another, rendering the rotation (β_1 and β_2) and tilt (Φ) angles significantly different from 180° . The unit cell is outlined with a broken blue line. Oxygen atoms are in blue. Distance (vertical green arrow) between (002) atomic planes (horizontal green lines) is also given. The octahedra are distorted such that basal (intraplane) Ru–oxygen distances R_1 and R_2 are different. Apical (out-of-plane) Ru–O distances R_3 and R_4 are also different.

remaining metallic. Then, an abrupt Mott-like transition takes place at $T_{\text{MIT}} = 48$ K to a near insulating phase [7, 12]. Earlier work has revealed that substituting Ti for Ru enhances the structural changes accompanying the metal-to-insulator transition (MIT) and, furthermore, significantly increases the temperature of PM-to-AFM phase transition [8, 13]. While the effect of external stimuli on the average crystal structure is still relevant, a likely key feature behind the enhancement is the emergence of lattice distortions leading to local variations in the crystal field strength [14]. Besides chemical substitution, the effect of other common external stimuli such as magnetic field and pressure on the electronic ground state structure of Ca ruthenates has also been related to emergent lattice distortions [15–17]. However, no systematic studies on

the character of the distortions have been conducted so far. Here we concentrate on revealing it by studying pure and Ti-substituted $\text{Ca}_3\text{Ru}_2\text{O}_7$ compounds using low temperature total x-ray scattering, including experiments in magnetic field. We find that the distortions occur not only in the individual bilayers but also involve bilayer–bilayer correlations, where the former increase with diminishing temperature and, similarly to the latter, diminish with magnetic field. Furthermore, we find that the local and average crystal lattice differ in terms of magnitude of the lattice distortions over a broad temperature range including the MIT. We argue that the distinct lattice distortions in pure and Ti-substituted $\text{Ca}_3\text{Ru}_2\text{O}_7$ may be viewed as their lattice degrees of freedom enabling the emergence of distinct electronic phases while the average crystallographic symmetry is preserved. Our findings highlight the importance of lattice distortions to the rich physics exhibited by strongly correlated transition metal oxides in general and in particular bilayer Ca ruthenates.

2. Experiment

Pure and 3% Ti-substituted $\text{Ca}_3\text{Ru}_2\text{O}_7$ crystals were grown using a floating zone [8]. In line with the findings of prior studies, in house x-ray diffraction (XRD) experiments showed that the crystals adopt an orthorhombic (S.G. $Bb2_1m$) structure. Electronic transport and thermal properties of the samples related to the MIT are reported in [8]. Results from magnetic measurements done on a physical property measuring system from Quantum Design are shown in figure 2. In line with the results of prior studies [5–13], both compounds are seen to undergo a PM-to-AFM transition at 55 K and 62 K while the MIT takes place at 48 K and 47 K, respectively. Hysteresis curves measured below the MIT confirm the presence of a metamagnetic phase transition in both compounds, where a ferromagnetic-like behavior is observed when the applied magnetic field reaches a critical value. For both pure and 3% Ti-substituted $\text{Ca}_3\text{Ru}_2\text{O}_7$, the field dependence of the magnetization appears linear above 70 K, as expected for PM materials.

Synchrotron XRD experiments were conducted at the beamline 28-ID-1 (PDF) at the National Synchrotron Light Source-II, Brookhaven National Laboratory using x-rays with energy of 74.46 keV ($\lambda = 0.1665$ Å). Samples were sealed in Kapton tubes and positioned inside a liquid He cryostat used to control their temperature. XRD data were obtained in transmission geometry, and scattered intensities were collected using an amorphous silicon PerkinElmer area detector. For each of the samples, data were taken over a temperature range from 300 K down to 10 K. Two data sets were obtained at each temperature point. One of the sets was obtained with the detector positioned 1000 mm away from the sample to achieve high resolution in reciprocal space necessary for Rietveld analysis described below. The other data set was obtained with the detector positioned 204 mm away from the sample to reach high wave vectors, q , ($q_{\text{max}} = 28$ Å⁻¹ in the current experiment) necessary to obtain high real space resolution atomic pair distribution functions (PDFs). The PDFs

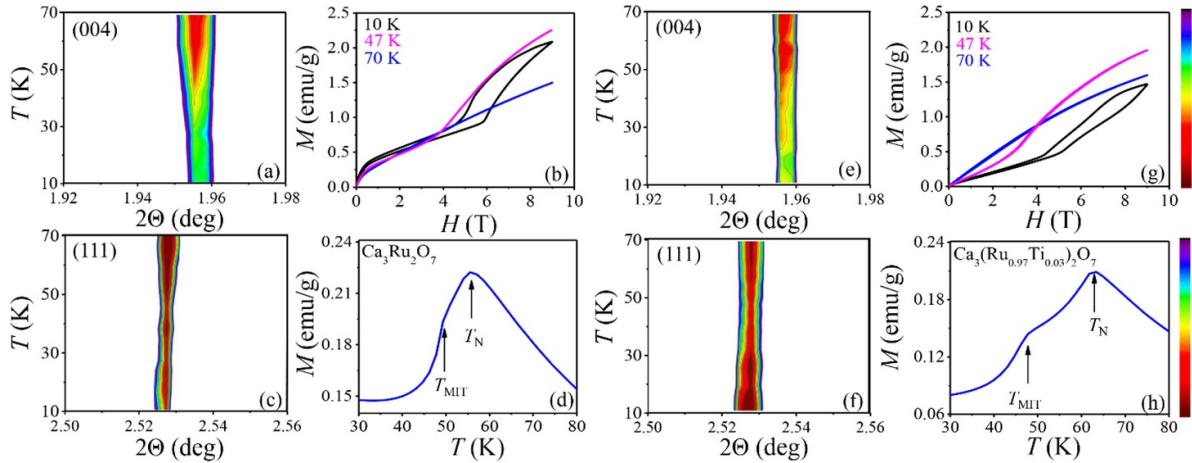


Figure 2. Selected Bragg peaks, labeled with their Miller indices, for (a), (c) pure and (e), (f) Ti-substituted $\text{Ca}_3\text{Ru}_2\text{O}_7$. The intensity of the peaks, in particular the (004) peak, changes markedly just below 50 K, reflecting the MIT transition. The paramagnetic (PM) metal to antiferromagnetic (AF) metal and MIT transitions, taking place at T_N and T_{MIT} , respectively, are clearly seen as inflection points in the magnetization data for (d) pure and (h) Ti-substituted $\text{Ca}_3\text{Ru}_2\text{O}_7$. Data in (b) and (g) show the presence of a metamagnetic phase transition in, respectively, pure and Ti-substituted $\text{Ca}_3\text{Ru}_2\text{O}_7$ when an external magnetic field in the order of 6 T is applied at a fixed temperature below the MIT (magenta and black curves). As it may be expected, magnetization data in (b) and (g) taken at 70 K (blue curves), i.e. at a temperature above the PM-to-AF transition, show a linear increase with the applied field, i.e. a behavior typical for PM materials. Note that the intensity of XRD peaks in (a), (e), (c), (f) increases as their color changes from blue towards dark red. The increase is at a constant rate, as indicated by the color bars on the right of the plot.

were derived from the XRD data following a well-established protocol [18]. Experimental XRD patterns for pure and Ti-substituted $\text{Ca}_3\text{Ru}_2\text{O}_7$ collected at different temperatures are summarized in figure S1 in terms of intensity color maps. Intensity color maps of the experimental PDFs are shown in Figure S2. For both samples, low temperature XRD patterns were also obtained in magnetic field with a strength of 5 T this time using x-rays with energy $E = 116.63$ keV ($\lambda = 0.1063$ Å). For the purpose, the samples were mounted on the tip of a cold finger attached to the cryostat and then inserted into the bore of an electromagnet.

3. Results and discussion

3.1. Average crystal structure

To reveal the temperature evolution of the average crystal lattice, the high q -resolution XRD data were subjected to Rietveld analysis [19] based on the known orthorhombic structure of $\text{Ca}_3\text{Ru}_2\text{O}_7$ [10]. In general, the fits, where lattice parameters, atomic positions and isotropic thermal factors were refined, reproduced the data well except the low-angle (002) and (004) Bragg peaks. Representative fits are given in figure S3. If the fits are repeated using a fixed value for the c parameter of the orthorhombic lattice directly derived from either (002) or (004) Bragg peaks, the latter are well fit but the fit to the remaining part of the XRD patterns deteriorates, as exemplified on figure S4. Moreover, values for the c lattice parameter obtained from (002) and (004) Bragg peaks appear different. The result shows that the periodicity of the crystal lattice in pure and Ti-substituted $\text{Ca}_3\text{Ru}_2\text{O}_7$ is disturbed in a direction perpendicular to the layers, likely due to disparities

in bilayer–bilayer stacking distances (\sim one half of c ; see figure 1) and distances between atoms at both sides of the bilayers (\sim one quarter of c) that are affected by the magnitude of octahedral tilts. Such a type of lattice distortion is typical for layered materials, including layered perovskites [20, 21]. The temperature evolution of a , b and c lattice parameters obtained through Rietveld fits and that for c lattice parameters directly derived from (002) and (004) Bragg peaks in the respective experimental XRD patterns are shown in figure 3. The evolution exhibits a discontinuity at the MIT, which is most noticeable with the c lattice parameters directly obtained from (002) Bragg peaks. The c lattice parameter obtained from (00 l) Bragg peaks in neutron diffraction patterns behaves similarly [13]. Concurrently, the unit cell volume increases slightly, which is also in line with the findings of previous studies [9, 10, 13].

3.2. Local crystal structure

To assess the distortions in the crystal lattice of pure and Ti-substituted $\text{Ca}_3\text{Ru}_2\text{O}_7$, we performed atomic PDF analysis that has proven useful in studies on crystals with intrinsic disorder [22, 23]. Representative atomic PDFs derived from XRD data obtained below and above the MIT, as fit [24] with a model based on the orthorhombic crystal structure of $\text{Ca}_3\text{Ru}_2\text{O}_7$, are given in figure 4. Similarly to the case of Rietveld fits, lattice parameters, atomic positions and isotropic thermal factors were refined in the PDF fits. As can be seen in figure 4 (left), an orthorhombic model that reproduces very well low- r PDF data, which reflect bonding distances within the unit cell (~ 20 Å), does not reproduce well the higher- r PDF data unless it is further refined against these data. The latter model, however, fails to reproduce well the low- r PDF data (see figure 4, right).

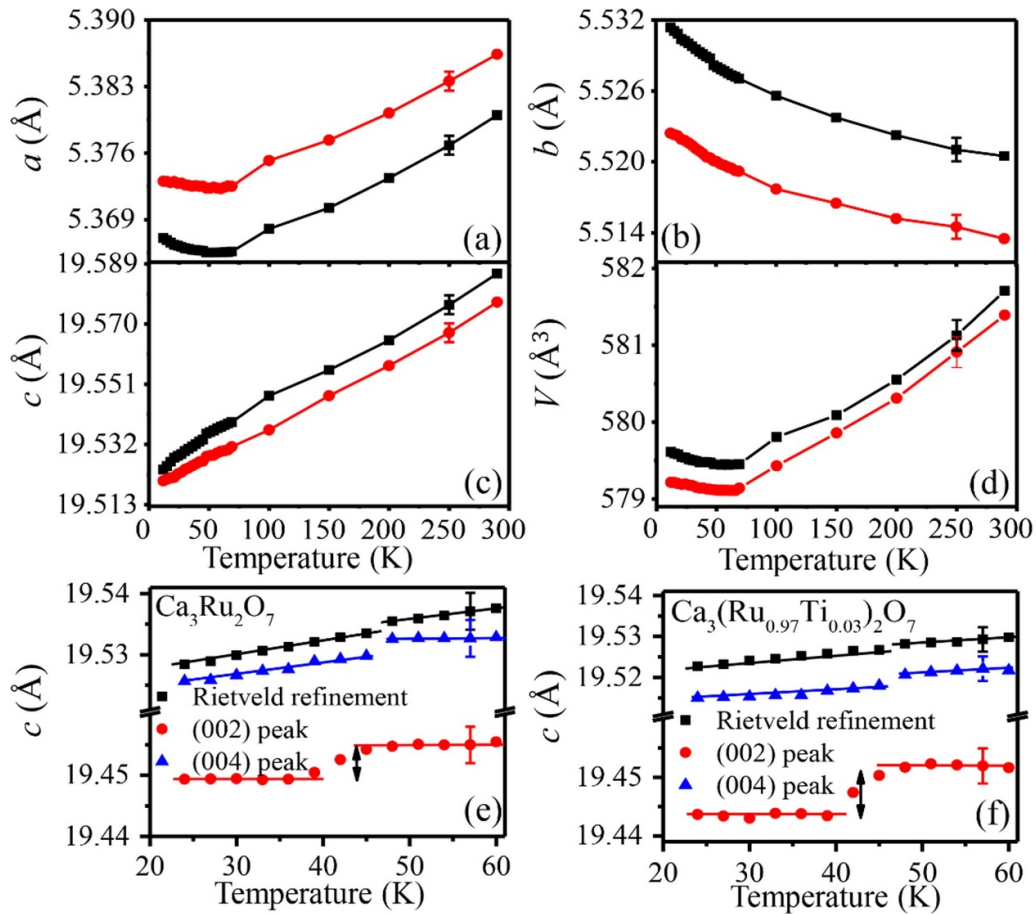


Figure 3. (a), (b), (c) Temperature evolution of Rietveld refined a , b and c lattice parameters and (d) unit cell volume, V , for pure (black squares) and Ti-substituted (red circles) $\text{Ca}_3\text{Ru}_2\text{O}_7$ over a broad temperature range. Temperature evolution of the c lattice parameter for (e) pure and (f) Ti-substituted $\text{Ca}_3\text{Ru}_2\text{O}_7$ in the vicinity of MIT as derived through Rietveld fits (black squares) and computed from the position of (002)/red dots and (004)/blue triangles Bragg peaks in the experimental XRD patterns. Black vertical arrows in (e), (f) highlight the presence of a discontinuity in the thermal evolution of c lattice parameter taking place at the MIT. Line through each set of data points is a guide for the eye. Data in (e) and (f) are summarized in table S1.

Orthorhombic lattice parameters a , b , and c and the so-called orthorhombicity parameter, γ , defined as $|a - b|/[0.5(a + b)]$, reflecting distortions in the octahedral bilayers are summarized in figure 5, as obtained from Rietveld fits and fits to low- r PDF data. Results in figures 4 and 5 show that the local and average crystal structure of nominally orthorhombic pure and Ti-substituted $\text{Ca}_3\text{Ru}_2\text{O}_7$ are not exactly the same, in particular in terms of bilayer distortions (γ values) and irregularities in the bilayer–bilayer separations. The magnitude of the latter can be conveniently assessed from the difference between c parameter values derived from Rietveld fits and such derived directly from (00 l) Bragg peaks.

To evaluate the difference as a function of length scale, we performed an extensive series of fits against PDFs obtained at different temperatures. In particular, for a given temperature, we refined the orthorhombic model against a sliding 10 Å window ranging from [1.5–10.5 Å] to [65.5–70.5 Å] in 5 Å steps, resulting in 14 fits per temperature. The results of each refinement represent the best-fit atomic structure on the length scale

set by the window, which is half of the crystallographic unit cell, i.e. equal to the bilayer–bilayer separation (see figure 1). Values for γ and c resulted from the refinements are shown in figure 6 for four representative temperatures. As can be seen in the figure, bilayer distortions and separation increase with interatomic distances and reach values characteristic to the average crystal structure at distances of about 30 Å that involve a stack of three perovskite bilayers. Data in figure 6 also show that the difference is preserved over a broad temperature range, including the MIT.

The origin of the spin lattice coupling in the ruthenates is associated with the orbital degree of freedom of Ru $4d$ electrons, which occupy four t_{2g} orbitals. Because Ti and Ru have the same valence state, i.e. Ti doping does not introduce additional charge carriers, changes in the electronic properties of both pure and Ti-substituted $\text{Ca}_3\text{Ru}_2\text{O}_7$, including the low-temperature transitions they undergo, may be expected to come largely from changes in the energy position and occupation of t_{2g}^4 orbitals. In turn, the latter are known to be highly

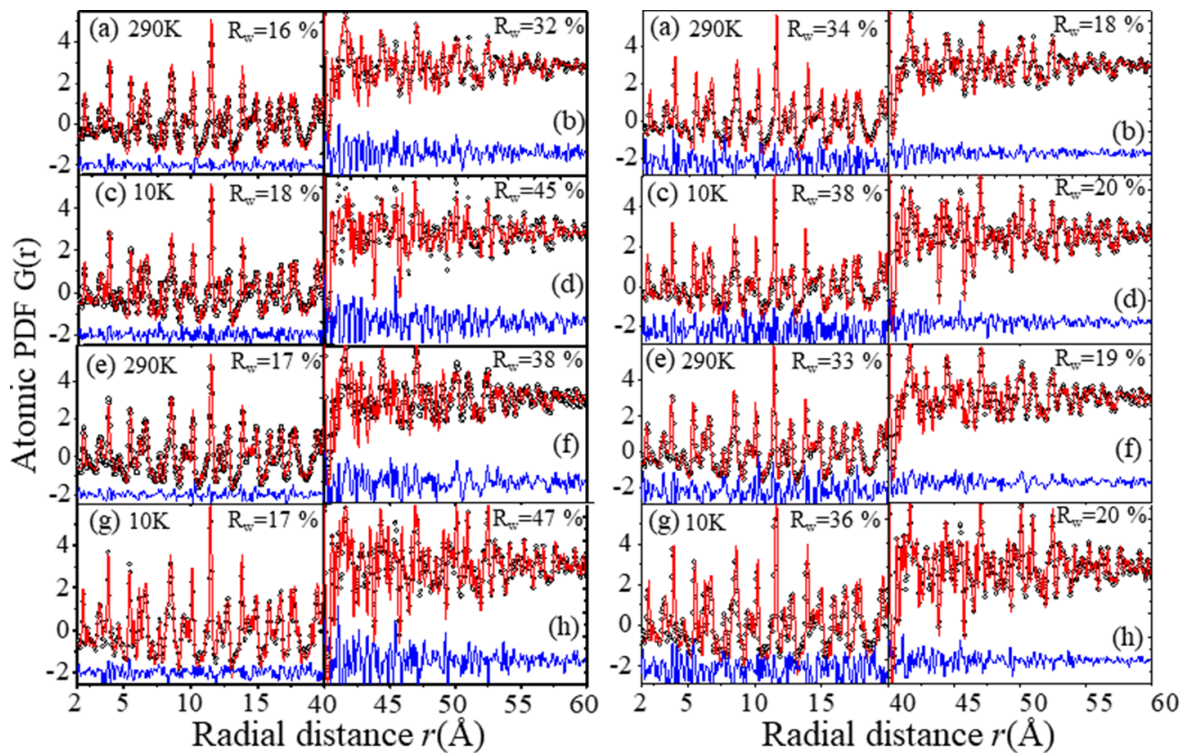


Figure 4. (Left panel) Successful orthorhombic (S.G. $Bb2_1m$) fits (red line) to the low- r part of experimental PDFs (symbols) for pure (a), (c) and Ti-substituted (e), (g) $\text{Ca}_3\text{Ru}_2\text{O}_7$ obtained at 290 K and 10 K. The residual difference (blue line) is shifted downward for clarity. Structure parameters resulted from the fits, however, cannot reproduce well the higher- r part of the PDFs, as shown in (b), (d) and (f), (h), respectively. (Right panel) Successful orthorhombic (S.G. $Bb2_1m$) fits to the high- r part of PDFs for pure (b), (d) and Ti-substituted (f), (h) $\text{Ca}_3\text{Ru}_2\text{O}_7$ obtained at 290 K and 10 K. Structure parameters resulted from the fits cannot reproduce well the low- r part of the PDFs, as shown in (a), (c) and (e), (g), respectively. The divergence between the nominally orthorhombic fits to low- r and high- r PDF data indicates that the local and average crystal structure of studied systems are significantly different.

dependent on the distortions of Ru-O_6 octahedra, involving in-plane octahedral rotations (β_1 and β_2 angles), out-of-plane tilting (Φ angles) and flattening [15, 16]. To evaluate the distortions, we computed the rotation and tilt angles defined in figure 1 both from Rietveld and PDF refined structure models. Results are shown in figure 7. As can be seen in the Figure, the magnitude of the rotations and tilting appears length scale dependent because their Rietveld (sensitive to the average crystal structure) and PDF (sensitive to the local crystal structure) derived values differ. We also computed Ru–O bonding distances and summarized the results in figure 8. In line with the findings of prior studies [10], data in the Figure show that the octahedral distortions in the studied systems change markedly at the MIT.

3.3. Influence of magnetic field

Due to strong spin–orbit interactions, pure and Ti-substituted $\text{Ca}_3\text{Ru}_2\text{O}_7$ are known to respond strongly to external magnetic field [7, 8, 12]. We collected XRD data in a constant field of 5 T in a temperature range extending from 70 K down to 20 K. For both compounds, Rietveld analysis of the data was successful both at low and high Bragg angles using a single value of the c lattice parameter (see figure S5). Refined

values of that parameter are summarized in figure 9 together with results from Rietveld analysis of XRD data collected in zero magnetic field. Also shown in the Figure are values for orthorhombicity derived from both sets of lattice parameters. As can be seen in the Figure, and in line with the findings of previous studies [15, 16], external magnetic field markedly changes the lattice parameters and orthorhombicity in both pure and Ti-substituted $\text{Ca}_3\text{Ru}_2\text{O}_7$, including their temperature evolution. From the Rietveld refined models, we also computed rotation and tilt angles of Ru-O_6 octahedra. Results are shown in figure 10. Data in figures 7 and 10 differ, indicating that magnetic field also affects the spatial orientation of Ru-O_6 octahedra. Moreover, it affects the octahedra flattening, as a comparison between out-of-plane Ru–O bonding distances shown in figures 8 and 11 indicates. Note, data in these Figures are computed from PDF refined models because, by definition, atomic PDFs directly reflect atomic pair distances.

4. Discussion

The MIT in pure and Ti-doped $\text{Ca}_3\text{Ru}_2\text{O}_7$ is accompanied by a moderate increase in the a and decrease in the b lattice parameter leading to an increase in the orthorhombic distortion

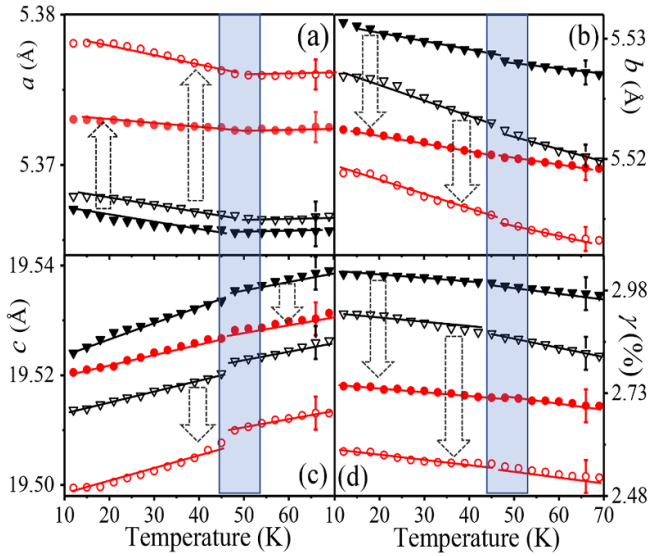


Figure 5. (a), (b) and (c) Temperature evolution of orthorhombic a , b and c lattice parameters for pure (solid black triangles) and Ti-substituted (solid red circles) $\text{Ca}_3\text{Ru}_2\text{O}_7$ as derived from Rietveld analysis. Same quantities derived from PDF analysis are shown as open black triangles and open red circles, respectively. (d) Values for orthorhombicity, γ , computed from the refined lattice parameters. All data sets exhibit a more or less expressed discontinuity at the MIT, highlighted by the vertical light blue rectangles. Dotted vertical arrows indicate the direction and magnitude of changes with Ti substitution. In particular, the b and c lattice parameters as well as orthorhombicity are seen to diminish with Ti substitution. The opposite is true for the a lattice parameter. Also, results from Rietveld and PDF analysis differ systematically, indicating the presence of a difference between the average and local crystal structure. Line through each set of data points is a guide for the eye. Data are summarized in tables S2 and S3.

of $(\text{CaRuO}_3)_2$ bilayers (see figures 3(a), (b) and 5(d)). Concurrently, a sharp decrease in the c lattice parameter takes place but the disparity between the c lattice parameters determined by (002)/(004) Bragg peaks and Rietveld fits, remains (see figures 3(e) and (f)). The disparity between in-plane rotations of Ru-O₆ octahedra sharing a common oxygen atom, as measured by the increased difference between β_1 and β_2 angles, also increases (figure 7). Just below the MIT, the octahedral tilts increase (Φ angles deviates further from 180°) and then decrease with further diminishing temperature, contributing to an overall twisting of the bilayers. Furthermore, the Ru-O₆ octahedra expand along the bilayers and flatten in a direction perpendicular to the layers, as indicated by the temperature evolution of basal and apical Ru-O bonding distances, respectively, shown in figure 8. It has been argued that tilting of Ru-O₆ octahedra would favor antiferromagnetic (AF) order. It has also been argued that the concurrent flattening and tilting of Ru-O₆ octahedra would lift the degeneracy of t_{2g} orbitals of Ru atoms by lowering the energy of d_{xy} orbitals relative to that of d_{yz} and d_{xz} orbitals, leading to orbital polarization such that xy orbitals in the down-spin channel are almost fully occupied and xz/yz orbitals are nearly empty, thus stabilizing the insulating ground state

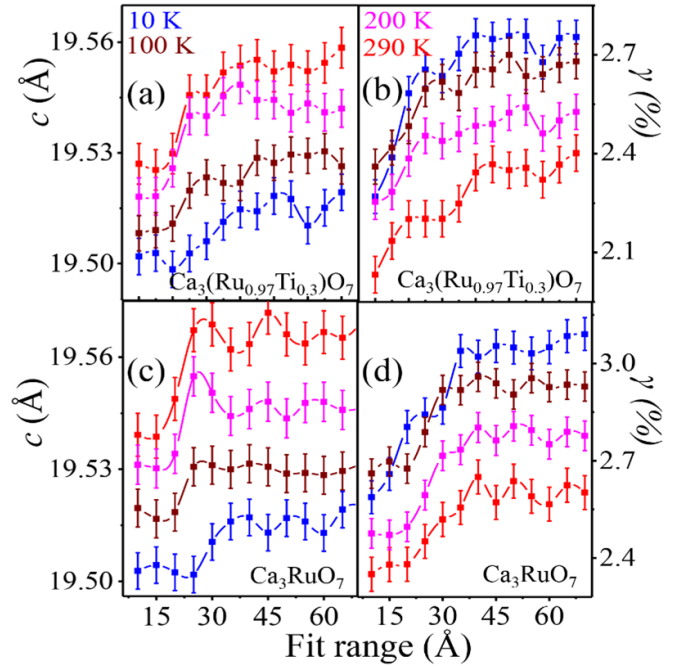


Figure 6. Orthorhombic (S.G. $Bb2_1m$) lattice parameter c resulted from a sequential, ‘box-car’-type refinement of atomic PDFs for (a) Ti-substituted and (c) pure $\text{Ca}_3\text{Ru}_2\text{O}_7$ obtained at a temperature of 100 K (brown), 200 K (magenta) and 290 K (red), which are above the MIT, and 10 K (blue), which is below the MIT. Data for orthorhombicity in Ti-substituted and pure $\text{Ca}_3\text{Ru}_2\text{O}_7$ obtained from the refinements are also shown in (b) and (d), respectively. In both compounds, bilayer distortions and bilayer-bilayer separation increase with interatomic distances over a broad temperature range. Also, as indicated by the diminished c lattice parameter, locally, i.e. for distances shorter than 30 Å, both compounds appear more compressed and with a reduced orthorhombicity in comparison to the bulk values derived from Rietveld fits and fits to higher- r PDF data. Line through each set of the data points is a guide to the eye.

[11, 13, 15]. Therefore, the insulating AF phase of $\text{Ca}_3\text{Ru}_2\text{O}_7$ appears to be promoted by increased overall orthorhombic distortion of $(\text{CaRuO}_3)_2$ bilayers (parameter γ), both frustrated and decreased bilayer separations, and increased distortions of Ru-O₆ octahedra. The strengthening of MIT taking place upon partially substituting Ti for Ru may be largely attributed to the increased flattening of Ru-O₆ octahedra, reflecting the steep shortening of basal Ru-O distances (see figure 8) and related increase in the discontinuity, Δc , of c lattice parameter ($\Delta c = 0.006$ Å in pure vs $\Delta c = 0.012$ Å in Ti-substituted $\text{Ca}_3\text{Ru}_2\text{O}_7$; see figure 3) taking place at the T_{MIT} .

Lastly, it may not come as a surprise that an external magnetic field of 5 T, which is known to destabilize the insulating phase, both increases the c lattice parameter and smooths its temperature evolution near the MIT. Concurrently, the orthorhombicity (figure 9), octahedral tilting and bilayer twisting (figure 10) appear decreased. Furthermore, both the flattening of Ru-O octahedra (compare the thermal evolution of apical Ru-O bonding distances in figures 8

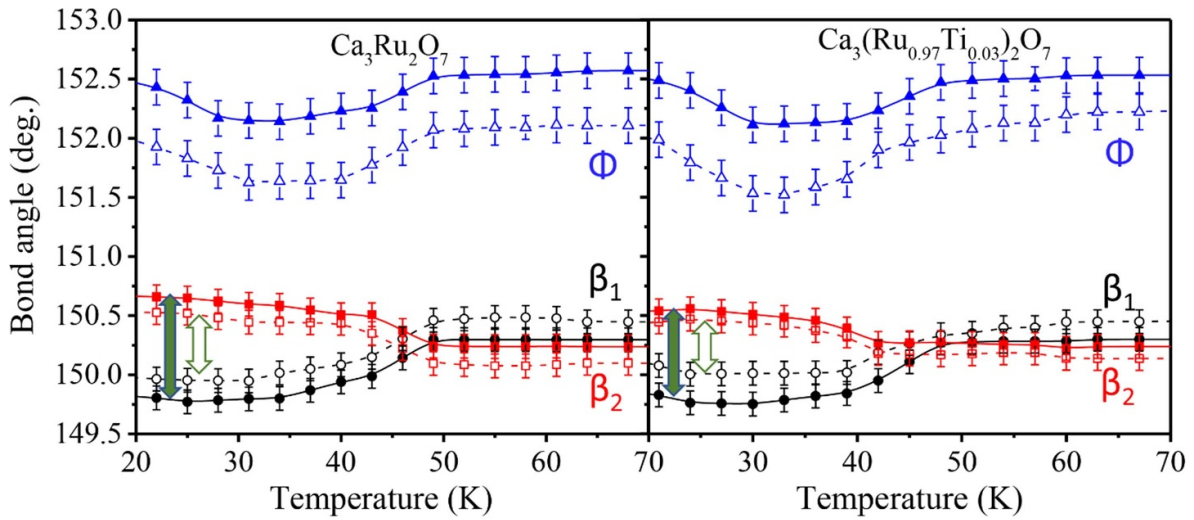


Figure 7. Temperature evolution of octahedral tilt (Φ) and rotation (β_1 and β_2) Ru–O–Ru angles in (left) pure and (right) Ti-substituted $\text{Ca}_3\text{Ru}_2\text{O}_7$. The angles are defined in figure 1. Solid symbols represent data derived from Rietveld fits and open symbols represent data derived from PDF fits, where both Rietveld and PDF fits are based on data obtained in zero magnetic field, respectively. The two rotation angles are close above MIT and seen to bifurcate below it whereas the tilt angle exhibits a broad undulation, rendering Ru–O bilayers twisted. Rietveld results are consistent with those reported in [10]. Notably, locally, the bilayer twisting appears decreased (open vs solid vertical arrows) and the octahedral tilting increased (Φ shifts further away from 180°) in comparison to those exhibited by the average crystal structure, as indicated by the divergence between Rietveld fit and PDF fit derived data. Also, pure and Ti-substituted $\text{Ca}_3\text{Ru}_2\text{O}_7$ show fine differences in the bilayer twisting and octahedral rotation. Line through each set of the data points is a guide to the eye.

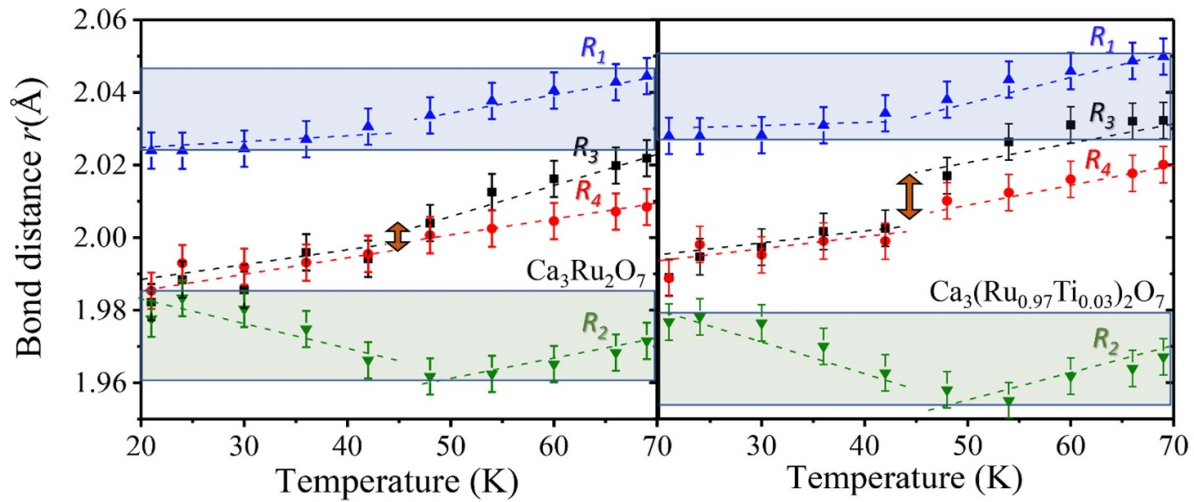


Figure 8. Temperature evolution of Ru–O bonding distances in (left) pure and (right) Ti-substituted $\text{Ca}_3\text{Ru}_2\text{O}_7$ derived from fits to PDFs obtained in zero magnetic field. Above MIT, the bonding distances show the usual uniform shrinking with diminishing temperature. Below MIT, the apical Ru–oxygen distances R_3 and R_4 drop (vertical arrows) and the basal distance R_1 hardly changes. By contrast, the basal distance R_2 increases with further diminishing temperature. The observed changes in Ru–O bonding distances signal a stretching and flattening of Ru–O₆ octahedra in a direction parallel and perpendicular to the bilayers, respectively. Furthermore, fine differences between Ru–O distances in pure and Ti-substituted $\text{Ca}_3\text{Ru}_2\text{O}_7$ are observed. In particular, R_1 distances in the former are systematically shorter than R_1 distances in the latter (compare the relative vertical displacement of the blue hatched rectangles that encompass the respective sets). The opposite is true for R_2 distances (compare the relative vertical displacement of the green hatched rectangles that encompass the respective data sets). Distances R_1 to R_4 are defined in figure 1. Line through each set of data points is a guide to the eye.

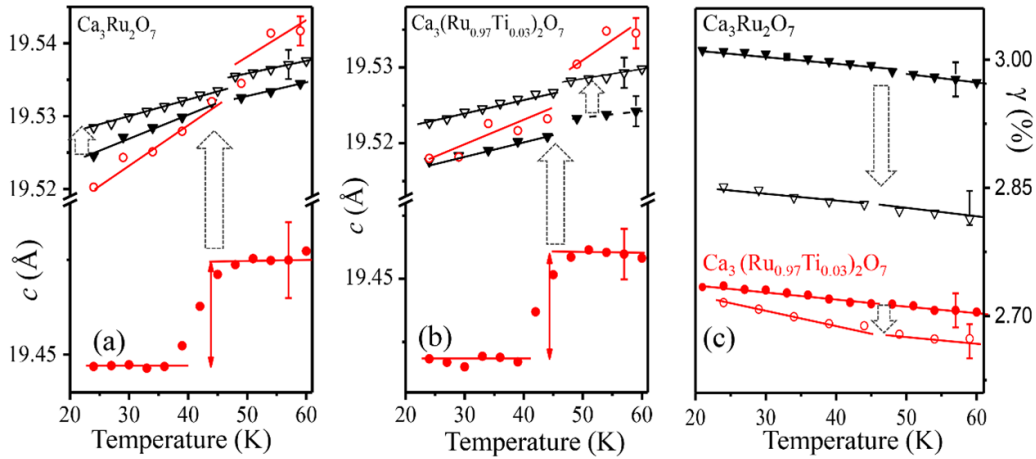


Figure 9. Comparison between c lattice parameters for (a) pure and (b) Ti-substituted $\text{Ca}_3\text{Ru}_2\text{O}_7$ derived from Rietveld fits to XRD data collected in zero magnetic field (solid black triangles) and in field with a strength of 5 T (open black triangles). Values for the c lattice parameter obtained from the position of the (002) Bragg peak in the respective XRD patterns are also shown as solid and open red circles, respectively. (c) Values for the orthorhombicity, γ , in pure and Ti-substituted $\text{Ca}_3\text{Ru}_2\text{O}_7$ computed from a and b lattice parameters derived from fits to PDFs obtained in zero magnetic field (solid triangles and circles) and in field with a strength of 5 T (open triangles and circles). Dotted arrows indicate the direction and magnitude of changes in the lattice parameter c and orthorhombicity when magnetic field is applied. In particular, the magnetic field is seen to diminish both the discontinuity in the c lattice parameter and orthorhombic distortion of bilayers of RuO_6 octahedra. Line through each set of the data points is a guide to the eye. Data are summarized in tables S4 and S5.

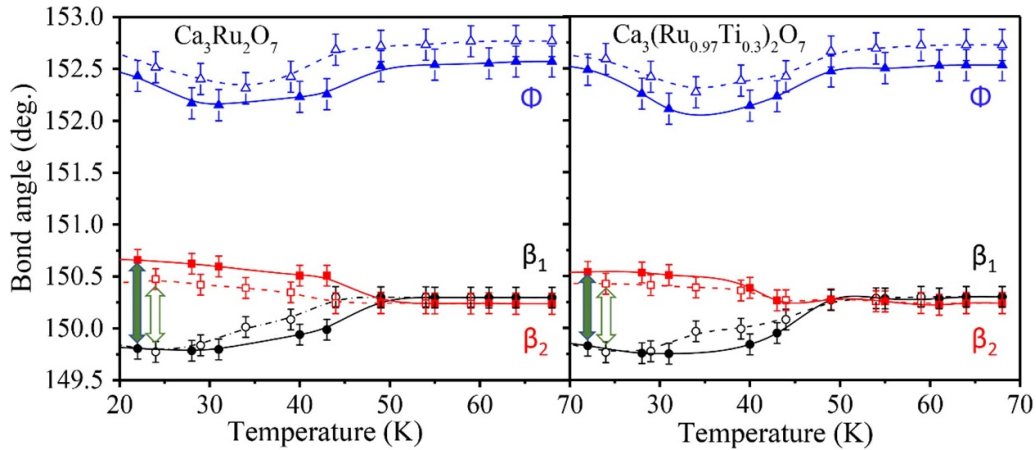


Figure 10. Temperature evolution of octahedral tilt (Φ) and rotation (β_1 and β_2) Ru–O–Ru angles in (left) pure and (right) Ti-substituted $\text{Ca}_3\text{Ru}_2\text{O}_7$. The angles are defined in figure 1. Solid symbols represent data derived from Rietveld refined XRD patterns collected in zero magnetic field. Open symbols represent data derived from Rietveld refined XRD patterns collected in magnetic field with a strength of 5 T. For both systems, octahedral tilts appear diminished (Φ shifts toward 180°) in magnetic field, favoring ferromagnetic type Ru–Ru exchange interactions. Furthermore, the degree of extra bilayer twisting, as measured by the difference between β_1 and β_2 values, appear diminished in magnetic field (open vertical arrow) in comparison to the case of no field (solid vertical arrow). Line through each set of data points is a guide to the eye.

and 11) and the disparity between the c lattice parameters obtained from (002)/(004) Bragg peaks and Rietveld fits appear diminished (figure 9), signaling a largely improved periodicity of the crystal lattice of corner shared octahedra in a direction perpendicular to the bilayers made of them (see figure 6). The observed field induced reduction of octahedral and lattice distortions would eventually lead to an orbital de-polarization, thus virtually ‘melting’ the Mott insulating phase. Depending on its strength, the field would also drive pure and Ti-substituted $\text{Ca}_3\text{Ru}_2\text{O}_7$ to a more or less ferromagnetic-like state, as shown in prior

studies [13, 15, 25, 26] and indicated by the observed here decrease in octahedral tilts. Notably, lattice distortions in both systems are ubiquitous, ranging from fine variations of bonding distances and angles (figures 5–8) to disrupted bilayer–bilayer correlations. Moreover, not only they have a distinct evolution as a function of temperature and magnetic field but also scale with interatomic distances, rendering the local and average crystal structure different. This may well explain the propensity of pure and Ti-substituted $\text{Ca}_3\text{Ru}_2\text{O}_7$ to adopt different structure states, each with distinct physical properties, in responding to different external stimuli.

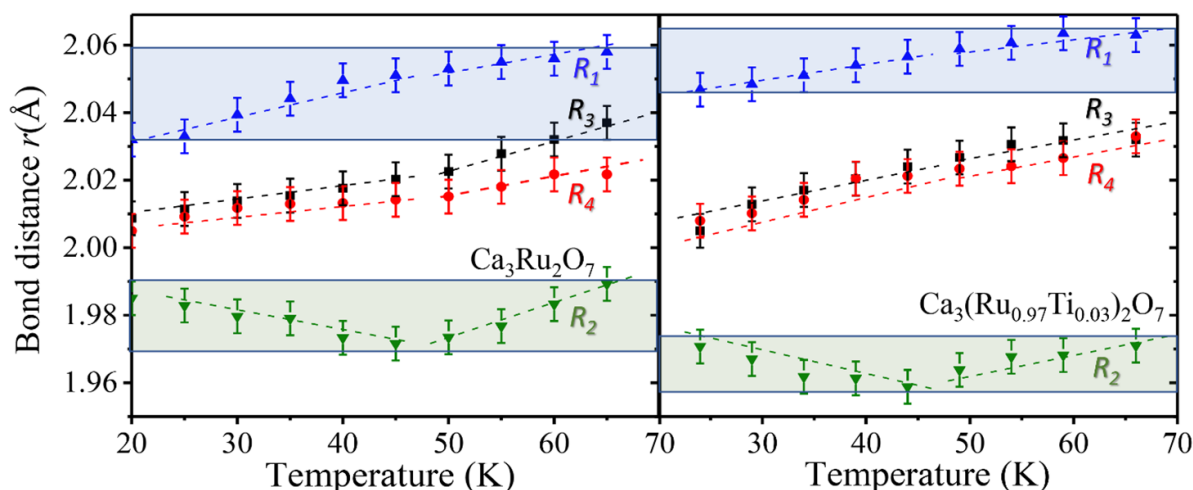


Figure 11. Temperature evolution of Ru–oxygen bonding distances in (left) pure and (right) Ti-substituted $\text{Ca}_3\text{Ru}_2\text{O}_7$ derived from fits to PDFs obtained in magnetic field with a strength of 5 T. Changes in apical Ru–oxygen bonding distances (R_3 and R_4) taking place at the MIT (at approx. 47 K) are much smaller than those observed in zero field (compare with data in figure 8). On the other hand, differences between R_1 distances in pure and R_1 distances in Ti-substituted systems appear increased in comparison to the case of no field (compare the relative vertical displacement of the blue rectangles here vs that of the blue rectangles in figure 8). The same is true for the difference between R_2 distances (compare the relative vertical displacement of the green rectangles here vs that of the green rectangles in figure 8). The results highlight the strong influence of magnetic field on the bonding distances and octahedral flattening in the studied systems. Distances R_1 to R_4 are defined in figure 1. Line through each set of the data points is a guide to the eye.

Simply, depending on the type and/or magnitude of particular stimulus, particular structural distortions would (dis)appear and corresponding electronic structure states (de)stabilized [7–9, 15, 16, 24, 25].

5. Conclusion

Our work illustrates the complex interplay between charge, spin and lattice degrees of freedom in bilayer ruthenates, where the lattice degrees of freedom indeed appear as distinct lattice distortions. Its major findings are (a) that not only the constituent octahedra and layers but also bilayer–bilayer correlations in these systems are intrinsically distorted, (b) the distortions coexist and interact on different length scales inevitably affecting charge transport and magnetic properties over both short and long-range distances, thus bridging proximal electronic phases with distinct ordered ground states.

Data availability statement

The data that support the findings of this study are available upon reasonable request from the authors.

Acknowledgments

This work was supported by the U S Department of Energy, Office of Science, Office of Basic Energy Sciences under Award No. DE-SC0021973 and used resources of the National Synchrotron Light Source at the Brookhaven National Laboratory provided by the DOE Office of Science under Contract No DE-SC0012704. The work at MSU was supported by the U S Department of Energy, Office of Science, Office of Basic

Energy Sciences, Materials Sciences and Engineering Division under DE-SC0019259. The work at PSU was supported by the US National Science Foundation under grant DMR 1917579.

ORCID iDs

V Petkov  <https://orcid.org/0000-0002-6392-7589>

E Fletcher  <https://orcid.org/0000-0003-0426-6570>

References

- [1] Tokura Y 2003 Correlated electron physics and transition metal oxides *Phys. Today* **56** 50
- [2] Morosan E, Natelson D, Nevidomsky A H and Si Q 2012 Strongly correlated materials *Adv. Mater.* **24** 4896
- [3] Marti K H and Reiher M 2011 New electron correlation theories for transition metal chemistry *Phys. Chem. Chem. Phys.* **13** 6750
- [4] McCusker J 2019 Electronic structure in the transition metal block and its implications for light harvesting *Science* **363** 484
- [5] Lei S *et al* 2018 Observation in quasi-2D polaron domains and ferroelastic switching in a metal $\text{Ca}_3\text{Ru}_2\text{O}_7$ *Nano Lett.* **18** 3088
- [6] Puchkov A V, Schabel M C, Basov D N, Startsev T, Cao G, Timusk T and Shen Z-X 1998 Layered Ru oxides. From band metal to Mott insulator *Phys. Rev. Lett.* **81** 2747
- [7] Cao G, McCall S, Crow J E and Guertin R P 1997 Observation of a metallic antiferromagnetic phase and metal to nonmetal transition in $\text{Ca}_3\text{Ru}_2\text{O}_7$ *Phys. Rev. Lett.* **78** 1751
- [8] Peng J, Ke X, Wan G, Ortmann J E, Fobes D, Hong T, Tian W, Wu X and Mao Z Q 2013 From quasi-two dimensional metals with ferromagnetic bilayers to Mott insulator with G-type antiferromagnetic order in $\text{Ca}_3(\text{Ru}_{1-x}\text{Ti}_x)\text{O}_7$ *Phys. Rev. B* **87** 085125

- [9] Markovic I *et al* 2000 Electronically driven spin-reorientation transition of the correlated polar metal $\text{Ca}_3\text{Ru}_2\text{O}_7$ *Proc. Natl Acad. Sci.* **117** 15524
- [10] Yoshida Y, Ikeda S, Matsuhara H and Shirakawa N Lee C and Katano C H 2005 Crystal and magnetic structure of $\text{Ca}_3\text{Ru}_2\text{O}_7$ *Phys. Rev. B* **72** 054412
- [11] Bartel Ch J, Sutton C, Goldsmith B R, Ouyang R, Musgrave Ch B, Ghiringhelli L M and Scheffler M 2019 New tolerance factor to predict stability of perovskite oxides and halides *Sci. Adv.* **5** eaav0693
- [12] Cao G, Balicas L, Xin Y, Crow J E and Nelson C S 2003 Quantum oscillations, colossal magnetoresistance, and the magnetoelastic interaction in bilayer $\text{Ca}_3\text{Ru}_2\text{O}_7$ *Phys. Rev. B* **67** 184405
- [13] Ke X, Peng J, Singh D J, Hong T, Tian W, Dela C R and Mao Z Q 2011 Emergent electronic and magnetic state in $\text{Ca}_3\text{Ru}_2\text{O}_7$ by Ti doping *Phys. Rev.* **84** 201102
- [14] Lechermann F, Han Q and Millis A 2020 Spatial inhomogeneity in $\text{Ca}_3(\text{Ru}_{1-x}\text{Ti}_x)\text{O}_7$ *Phys. Rev. Res.* **2** 033490
- [15] Zhu M, Peng J, Zou T, Prokes K, Mahanti S D, Hong T, Mao Z Q, Mao G Q, Liu G Q and Ke X 2016 Colossal magnetoresistance in a Mott insulator via magnetic field driven insulator-metal transition *Phys. Rev. Lett.* **116** 216401
- [16] Zhao H, Zhen H, Terzic J, Son W, Ni Y, Zhang Y, Schlottmann P and Cao G 2021 Lattice instability in $\text{Ca}_3\text{Ru}_2\text{O}_7$: control of electrical transport via anisotropic magnetostriction *Phys. Rev. B* **104** L121119
- [17] Ramires A and Sigrist M 2016 Identifying of detrimental effects for multiorbital superconductivity: application to Sr_2RuO_4 *Phys. Rev. B* **94** 104501
- [18] Yang X, Juhas P, Farrow C L and Billinge S J L 2013 PDFgetX3: a rapid and highly automatable program for processing powder diffraction data into total scattering pair distribution functions *J. Appl. Crystallogr.* **46** 560
- [19] Toby B H and Von Dreele R B 2013 GSAS-II: the genesis of a modern open-source all-purpose crystallography software package *J. Appl. Crystallogr.* **46** 544
- [20] Kalantar-Zadeh K, Ou J Z, Daeneke T, Mitchell A, Sasaki T and Fuhrer M S 2016 Two dimensional and layered transition metal oxides *Appl. Mater. Today* **5** 73
- [21] Schaak R E and Mallouk T E 2002 Perovskites by design: a toolbox of solid-state reactions *Chem. Mater.* **14** 1455
- [22] Petkov V 2008 Nanostructure by high-energy x-ray diffraction *Mater. Today* **11** 28
- [23] Egami T and Billinge S J L 2003 *Underneath the Bragg's Peaks* Pergamon Materials Series vol 7 (Amsterdam: Pergamon Press) ([https://doi.org/10.1016/S1369-7021\(03\)00635-7](https://doi.org/10.1016/S1369-7021(03)00635-7))
- [24] Farrow C L, Juhas P, Liu W, Bryndin D, Bozin E S, Bloch J, Proffen T and Billinge S J L 2007 PDFfit2 and PDFgui: computer program to study nanostructure in crystals *J. Phys.: Condens. Matter* **19** 335219
- [25] McCall S, Cao G and Crow J E 2003 Impacts of magnetic fields on anisotropy in $\text{Ca}_3\text{Ru}_2\text{O}_7$ *Phys. Rev. B* **67** 094427
- [26] Bao W, Mao Z Q, Qu Z and Lynn J W 2008 Spin-valve effect and magnetoresistivity in single crystalline $\text{Ca}_3\text{Ru}_2\text{O}_7$ *Phys. Rev. Lett.* **100** 247203